

Deformation Mechanism Analysis of Three-Roller Continuous and Synchronous Calibration Process of Straightness and Roundness For LSAW Pipes

Xueying Huang

Ningbo University of Finance and Economics

Gaochao Yu (✉ gch_yu@ysu.edu.cn)

Yanshan University

Chunge Wang

NingboTech University

Jun Zhao

Yanshan University

Research Article

Keywords: LSAW pipes, Three-roller, Continuous and synchronous calibration process, Deformation mechanism, Numerical simulations, Axial and circumferential bidirectional reciprocating bending

Posted Date: November 12th, 2021

DOI: <https://doi.org/10.21203/rs.3.rs-1057310/v1>

License:  This work is licensed under a Creative Commons Attribution 4.0 International License.

[Read Full License](#)

Deformation mechanism analysis of three-roller continuous and synchronous calibration process of straightness and roundness for LSAW pipes

Xueying Huang^a, Gaochao Yu^{b,*}, Chungue Wang^c, Jun Zhao^b

^a *School of Digital Technology and Engineering, Ningbo University of Finance and Economics, Ningbo City, PR China, 315175*

^b *Key Laboratory of Advanced Forging & Stamping Technology and Science (Yanshan University), Ministry of Education of China, Qinhuangdao City, PR China, 066004*

^c *School of Mechanical and Energy Engineering, NingboTech University, Ningbo City, PR China, 315100*

* Corresponding Author. Address: College of Mechanical Engineering, Yanshan University, No.438, Hebei Street, Haigang District, P.O.Box 066004, Qinhuangdao, P.R. China.

E-mail: huangxueying@nbufe.edu.cn (X. Huang), gch_yu@ysu.edu.cn (G. Yu), wangchunge@nbt.edu.cn (C. Wang), zhaojun@ysu.edu.cn (J. Zhao)

Abstract: Continuous and synchronous calibration process of straightness and roundness for LSAW (Longitudinally Submerged Arc Welding, LSAW) pipes with three rollers is a bidirectional reciprocating bending process that includes axial and circumferential directions. It is particularly important to reveal the deformation mechanism, which provides theoretical support for the calibration process to be applied to actual production. Based on this, through the combination of references, theoretical analysis and numerical simulation, the deformation mechanism is analyzed in this paper. The whole deformation process of pipe is modeled and then numerically simulated with FEM software of ABAQUS. The results show that reciprocating bending can eliminate the difference of initial curvature, so that the axial curvature and circumferential curvature are unified to the same direction and value respectively. The synergy between the axial reciprocating bending straightening process and the circumferential reciprocating bending rounding process realizes the calibration process of LSAW pipes. The simulation results support the theoretical results, and the deformation is mainly caused by axial stress and circumferential stress.

Keywords: LSAW pipes; Three-roller; Continuous and synchronous calibration process; Deformation mechanism; Numerical simulations; Axial and circumferential bidirectional reciprocating bending

Highlights:

1) Through the combination of references, theoretical analysis and numerical simulation, the deformation mechanism of the calibration process has been analyzed.

2) The deformation mechanism analysis provides theoretical guidance for the application of the process to actual production.

3) The analysis method provides a new idea for simplifying the problem of three-dimensional deformation.

1 Introduction

With the development of the world's oil and gas resources transferring to unconventionality, remote and harsh development environment and the development trend of oversized transmission have put forward higher requirements for pipeline construction. Longitudinally Submerged Arc Welding (LSAW) pipes are made from high-steel wide plates, especially for long-distance oil and gas pipeline transportation and for laying pipes in deep-sea or cold areas. The straightness and roundness of formed welding pipe cannot meet the industrial standards due to the factors such as welding thermal stress, material properties and technical equipment[1-3]. Therefore, the formed welding pipe needs to be straightened and rounded (the process of straightening and rounding is referred to as the calibration process in this paper). According to the American Petroleum Institute's industry standard ANSI/API Spec. 5L, the straightness and roundness finished welding pipes have been strictly required. The roundness of the finished welding pipe does not exceed $\pm 0.75\%$ of the nominal outer diameter, and the straightness is not greater than 0.2% of the total length of the pipe [4].

At present, the roundness calibration process mainly includes the whole-diameter roundness calibration process[5,6], the over-bending roundness calibration process[7-9], and the roll-type roundness calibration process[10-12]. Common straightness calibration techniques include the pressure straightening [13-15] and the cross roll straightening [16-19]. The existing roundness and straightness calibration processes are done separately. On the one hand, it leads to the growth of production process and the reduction of production efficiency, which is not easy to realize

automatic and intelligent production; On the other hand, because the deformation affect each other, the flattening problem of LSAW pipes cannot be solved [20]. It is difficult to adjust both the straightness and roundness to optimal levels, which also seriously affects on-site welding and pipeline safety [21]. In view of the application trend of LSAW pipes and the existing problem of calibration technology, a new three-roller continuous and synchronous calibration process of straightness and roundness was proposed [21-24]. The study of process deformation mechanism provides theoretical support for understanding the essence of process and applying it to actual production.

Based on the combination of reference, theoretical analysis and numerical simulation, this paper further studies the deformation mechanism of the calibration process. It includes the axial reciprocating bending straightening process and the circumferential reciprocating bending rounding process. In addition, the distribution of equivalent stress, maximum and minimum principal stress of pipe in Section III is analyzed; The effects of axial stress, circumferential stress and radial stress on pipe deformation are discussed. The simulation results can support the theoretical analysis results.

2 Process introduction

The three-roller continuous and synchronous calibration process of straightness and roundness for LSAW pipes is shown in Fig. 1. The process' main working parts are three parallel rollers, including a convex roller (upper roller) and two concave rollers (lower rollers). Before experiment, each roller pushes the same radial reduction towards the pipe's central axis. During the experiment, two concave rollers rotate simultaneously driven by servo motors. This makes the pipe and convex roller rotate under the action of friction. At the same time, the servo motor drives the push plate to make the pipe move along the slideway, thus finishing the calibration process.

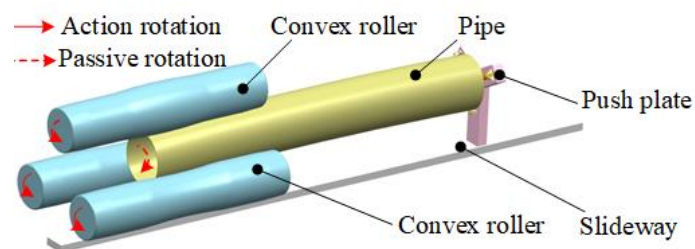
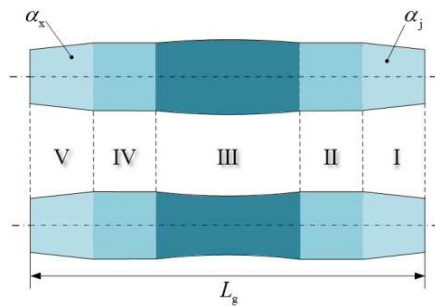


Fig. 1 Schematic diagram of the calibration process

The schematic diagram of roller-shape is shown in Fig. 2. As shown in Fig. 2, both ends of the roller are loading section (Section I) and unloading section (Section V), both of which are truncated cone shape. The design enables the pipe to enter smoothly between the three rollers and ensures that the pipe can unload smoothly, so as to unify the curvature. Section II and Section IV are roundness calibration sections, which are cylindrical in shape. The design can make the pipe undergo multiple reciprocating bending along the circumferential direction, resulting in elastic-plastic deformation. Thus, roundness calibration and complementary roundness calibration are realized. Section III is roundness and straightness calibration section. The upper roller part is convex and the lower roller part is concave. The design ensures that the pipe can undergo multiple reciprocating bending along the circumferential and axial directions. Thereby, roundness and straightness calibration are realized.



Section I: Loading section; Section II: Roundness calibration section; Section III: Roundness and straightness calibration section; Section IV: Roundness complement calibration section; Section V: Unloading section

Fig. 2 Schematic diagram of roller-shape

The curvature distribution of Section III is shown in Fig. 3. Section III is composed of n tangent arcs with changing curvature, whose curvature is gradually reduced from the middle to both ends. That is, K_1 to K_n gradually increases in value, and K_n is the maximum curvature of Section III.

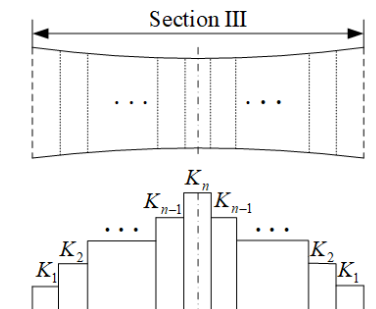


Fig. 3 Curvature distribution of Section III - n -segment curvature

Fig. 4 is a schematic diagram of the loading parameter. Three rollers load the same radial reduction toward the pipe center, and the stroke of each roller is recorded as H .

$$H = R_1 + R - H_j \quad (1)$$

where H is the radial reduction, R_1 is the roller radius, R is the pipe radius, H_j is the distance from the pipe's center to the center of roller after loading.

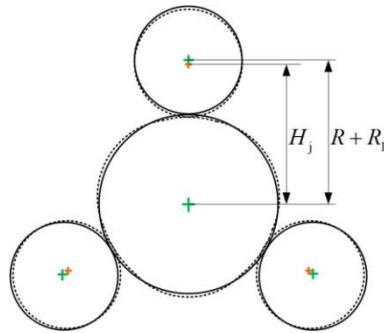


Fig. 4 Diagram of loading parameters

3 Process deformation mechanism

In this paper, the axial and circumferential reciprocating bending deformation are simplified to the pure bending problem of plane curved beam[25].

3.1 Reciprocating bending springback analysis of axial straightening

The straightening process of the calibration process is an axial reciprocating bending process. As shown in Fig. 3 above, the curvature distribution of Section III is constantly changing, with the curvature increasing from zero (K_1) to K_n and then reduced to zero. According to the geometric characteristics of LSAW pipe, a linear simple kinematic hardening (LSKH) constitutive model is adopted [16], as shown in Fig. 5.

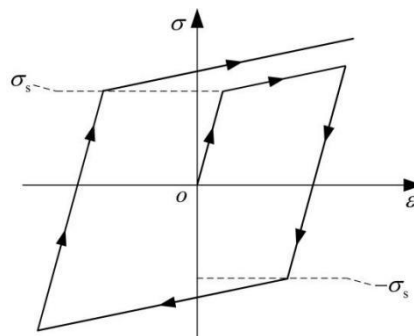


Fig. 5 LSKH constitutive model

The expression is as follows

$$\sigma = \begin{cases} D\varepsilon + \sigma_0 & \varepsilon > 0 \\ D\varepsilon - \sigma_0 & \varepsilon < 0 \end{cases} \quad (2)$$

$$\sigma_0 = \left(1 - \frac{D}{E}\right)\sigma_s$$

where σ_s is yield stress, D is plastic modulus, E is elastic modulus.

The circular section of pipe is shown in Fig. 6. The coordinate system is established with the geometric center of the section as the coordinate origin. The bending moment M during loading can be simply described as

$$M = \int_A \sigma z dz = \begin{cases} DI(K - K_0) + M_0 & K \geq K_0 \\ DI(K - K_0) - M_0 & K < K_0 \end{cases} \quad (3)$$

where, $M_0 = \frac{4\sigma_0}{3}(R_1^3 - R_2^3)$, $I = \frac{\pi}{4}(R_1^4 - R_2^4)$, R_2 is the inner diameter of pipe.

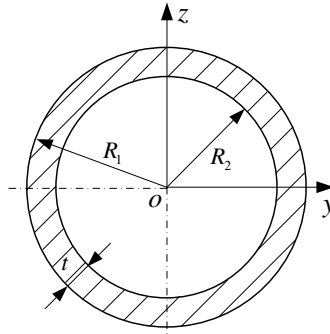


Fig. 6 Circular section of pipes

Since the deformation of each section is continuous, the current initial curvature can be used as the curvature after the last bending springback. According to Eq. (3), the recurrence equation of reciprocating bending can be expressed as

$$K_{pn} = \begin{cases} K_1 - \frac{M_1(K_1, K_0)}{EI} & n = 1 \\ K_n - \frac{M_n(K_n, K_{p(n-1)})}{EI} & n \geq 2 \end{cases} \quad (4)$$

where, n is the times of reciprocating bending, K_{pn} is the springback curvature after reciprocating bending n times.

Based on the springback theory of small curvature plane bending [26], the springback

curvature of pipe micro beam after reciprocating bending n times along the axis is deduced by mathematical induction. The reciprocating bending process is shown in Fig. 7.

If the first bending is reverse bending, the unified equation of curvature after springback is

$$K_{pn} = K_n - \frac{D}{E}(K_n - K_{n-1}) - \left(\frac{D}{E}\right)^2 (K_{n-1} - K_{n-2}) - \dots - \left(\frac{D}{E}\right)^{n-1} (K_2 - K_1) + (-1)^{n+1} \left(\frac{16\sigma_0 (R_1^3 - R_2^3)}{3\pi (R_1^4 - R_2^4)(E + D)} \right) \quad (5)$$

If the first bending is positive bending, the unified equation of curvature after springback is

$$K_{pn} = K_n - \frac{D}{E}(K_n - K_{n-1}) - \left(\frac{D}{E}\right)^2 (K_{n-1} - K_{n-2}) - \dots - \left(\frac{D}{E}\right)^{n-1} (K_2 - K_1) + (-1)^n \left(\frac{16\sigma_0 (R_1^3 - R_2^3)}{3\pi (R_1^4 - R_2^4)(E + D)} \right) \quad (6)$$

Eqs. (5) and (6) can be expressed uniformly as

$$\bar{K}_{pn} = f(D, E, \sigma_0, R_1, R_2, K_1, K_2, \dots, K_n) \quad (7)$$

Eq. (7) proves that multiple reciprocating bending can eliminate the difference of initial curvature along the axial direction and unify the curvature to the same direction and value. \bar{K}_{pn} is related to material properties, inner and outer diameter of pipe and bending curvature. When the loading curvature K_n tends to zero, the springback curvature along the axial direction of the pipe after reciprocating bending is also close to zero, thus achieving straightening.

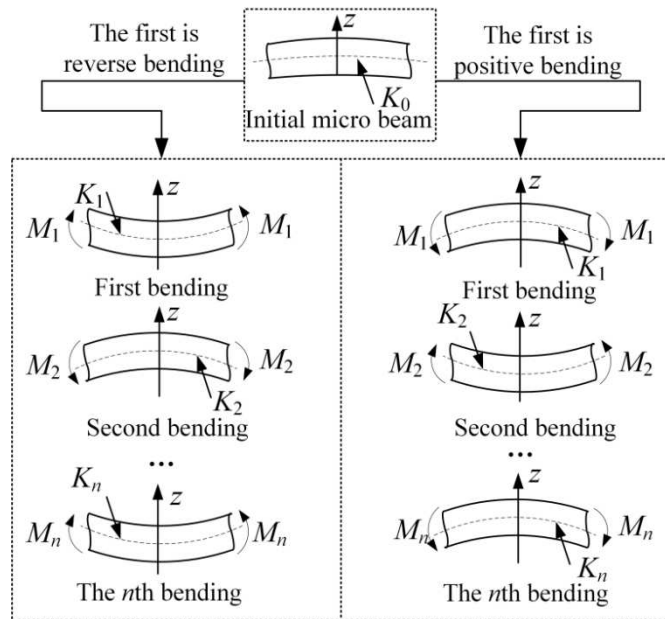


Fig. 7 Schematic diagram of reciprocating bending of micro-beam

3.2 Reciprocating bending springback analysis of circumferential rounding

The rounding process of the calibration process is a circumferential reciprocating bending process. Similarly, a linear simple kinematic hardening (LSKH) constitutive model is adopted [16]. The relation of the bending moment and the curvature can be described as

$$M = \int_A \sigma z dz = \begin{cases} DI(K - K_0) + M_0 & K \geq K_0 \\ DI(K - K_0) - M_0 & K < K_0 \end{cases} \quad (8)$$

where, $M_0 = \frac{\sigma_0 t^2}{4}$.

Then, the springback curvature of pipe micro beam after reciprocating bending n times along the circumferential direction is deduced. The reciprocating bending process is shown in Fig. 7. The derivation process is the same as that of axial reciprocating bending.

If the first bending is reverse bending, the unified equation of curvature after springback is

$$K_{pn} = K_n - \frac{D}{E}(K_n - K_{n-1}) - \left(\frac{D}{E}\right)^2 (K_{n-1} - K_{n-2}) - \dots \\ - \left(\frac{D}{E}\right)^{n-1} (K_2 - K_1) + (-1)^{n+1} \frac{3\sigma_0}{t(E+D)} \quad (9)$$

If the first bending is positive bending, the unified equation of curvature after springback is

$$K_{pn} = K_n - \frac{D}{E}(K_n - K_{n-1}) - \left(\frac{D}{E}\right)^2 (K_{n-1} - K_{n-2}) - \dots \\ - \left(\frac{D}{E}\right)^{n-1} (K_2 - K_1) + (-1)^n \frac{3\sigma_0}{t(E+D)} \quad (10)$$

Eqs. (9) and (10) can be expressed uniformly as

$$\bar{K}_{pn} = f(D, E, \sigma_0, t, K_1, K_2, \dots, K_n) \quad (11)$$

Eq. (11) proves that multiple reciprocating bending can eliminate the difference of initial curvature along the circumferential direction and unify the curvature to the same direction and value. \bar{K}_{pn} is related to material properties, thickness of pipe-wall and bending curvature. When the loading curvature K_n tends to a certain value, the springback curvature along the circumferential direction of pipe after reciprocating bending tends to be consistent, thus achieving rounding.

4 Numerical simulation

Using the software ABAQUS, a finite element model of the LSAW pipe calibration process is

established, as shown in Fig. 8. Regardless of the effect of pipe welds on the continuous calibration process, the mechanical properties and geometric dimensions of pipes are shown in Table 1 and the geometric dimensions of rollers is shown in Table 2. The pipe is set as a deformable body. The pipe-wall is divided into 4 layers along the thickness, and the pipe is discretized by 8-node linear hexagonal nonconforming mode elements. Select the continuum distributing coupling method to couple the center point of the pipe cross-section and the pipe cross-section boundary, and select all 6 degrees of freedom for the constrained area. The three rollers are set as discrete rigid bodies. The contact between the pipe and each roller is set to pure master-slave contact and motion contact conditions, and the coefficient of friction is 0.2.

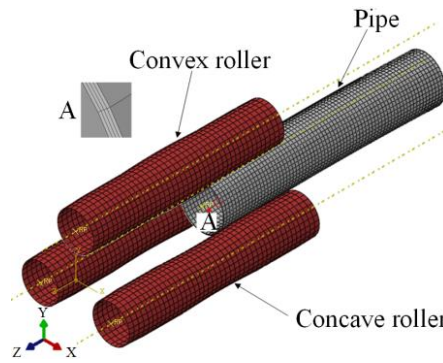


Fig. 8 Finite element model

Table 1 Mechanical properties and geometric dimensions of pipes

| Material | Elastic modulus E (GPa) | Yield stress σ_s (MPa) | Plastic modulus D (MPa) | Outer diameter D_p (mm) | Length L_p (mm) | Thickness t (mm) | Initial roundness | Initial straightness |
|----------|------------------------------|----------------------------------|------------------------------|------------------------------|----------------------|--------------------|-------------------|----------------------|
| ST12 | 179 | 189 | 1500 | 140 | 700 | 2 | 5% | 10‰ |

Table 2 Geometric dimension of rollers

| Outer diameter D_g (mm) | Length L_g (mm) | Proportion of rollers | Taper of Section I (rad) | Taper of Section V (rad) | K_n (mm^{-1}) | Roller shape curve of Section III |
|------------------------------|----------------------|-----------------------|--------------------------|--------------------------|----------------------------|-----------------------------------|
| 120 | 600 | 1:2:4:2:1 | 0.033 | 0.025 | 0.001 | $0.16x^2 - 0.0004y^2 - 1 = 0$ |

5 Results and discussion

In the numerical simulation, the roller rotation speed is 150 mm/s and the pipe forward speed

is 4mm/s. The times of reciprocating bending of ST12 pipe from starting to contact the roller to completely separating from the roller is 67.

The equivalent stress distribution of one-half ST12 pipe in Section III is shown in Fig. 9. According to the symmetry, there are three positive bending regions and three reverse bending regions along the circumferential direction. They are evenly distributed in the whole pipe [22].

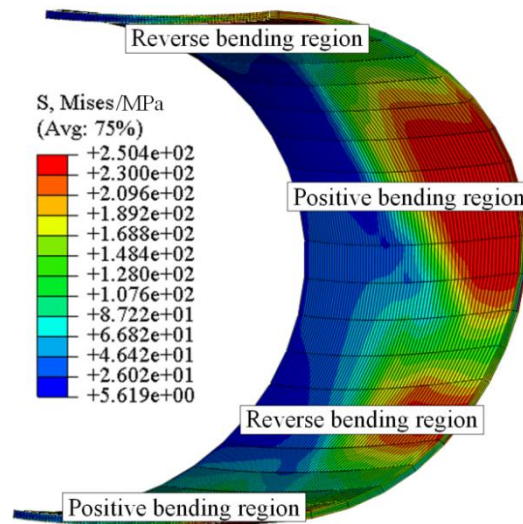
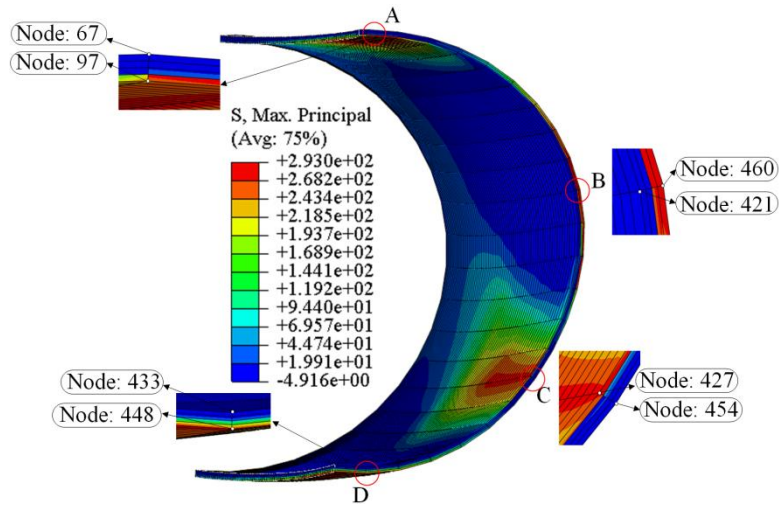
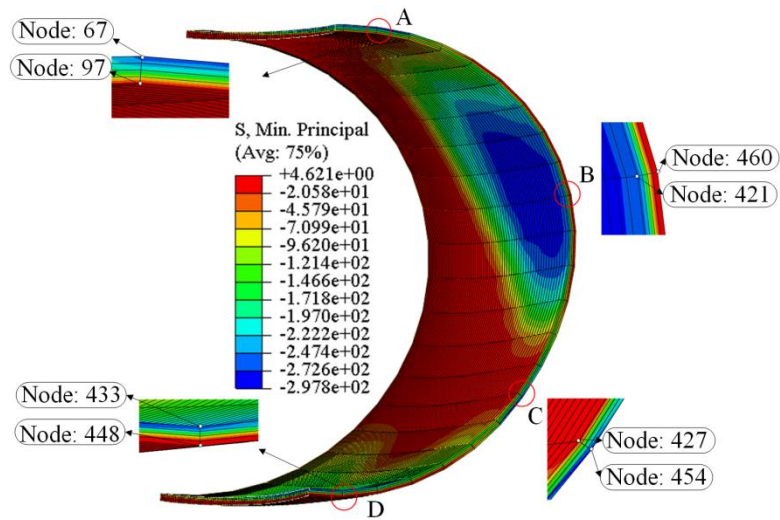


Fig. 9 Equivalent stress distribution of one-half pipe

The distribution of maximum and minimum principal stress in Section III is shown in Fig. 10. The maximum and minimum principal stress values are shown in Table 3. In combination with Figs. 9 and 10, it can be seen that positions A and C are located in the reverse bending region. The maximum principal stress is generated in the inner layer of the pipe (nodes 97 and 427), and the minimum principal stress is generated in the outer layer of the pipe (nodes 67 and 454). Positions B and D are located in the positive bending region. The maximum principal stress is generated in the outer layer of the pipe (nodes 460 and 448), and the minimum principal stress is generated in the inner layer of the pipe (nodes 421 and 433). Based on the above analysis, the absolute values of the maximum principal stress and the minimum principal stress of the pipe any position are basically equal, which verifies the characteristics of pure bending deformation.



(a) Maximum principal stress



(b) Minimum principal stress

Fig. 10 Distribution of maximum and minimum principal stress

Table 3 Maximum and minimum principal stress

| Position | Node ID | Maximum principal stress /MPa | Minimum principal stress /MPa |
|----------|---------|-------------------------------|-------------------------------|
| A | 67 | — | -257 |
| | 97 | +251 | — |
| B | 460 | +282 | — |
| | 421 | — | -281 |
| C | 454 | — | -286 |
| | 427 | +285 | — |
| D | 448 | +277 | — |
| | 433 | — | -269 |

The distribution of axial stress along the thickness and length directions in Section III is

shown in Fig. 11. Under the influence of axial stress, plastic deformation occurs along the thickness and length directions. It is proved that the geometric dimension of the longitudinal section of the pipe has changed.

Fig. 11 (a) shows the distribution of axial stress along the thickness direction. In the positive bending region, the pipe's outer layer is stretched with a maximum stress of 249 MPa (node 5) and a minimum stress of 0 MPa (node 1); In the reverse bending region, the inner layer of the pipe is compressed with a maximum stress of 0 MPa (node 5) and a minimum stress of -278 MPa (node 1). The above indicates that one part of the pipe-wall has reached yield strength, while the other part has produced only elastic deformation.

Fig. 11 (b) shows the distribution of axial stress along the length direction. The axial stress of the pipe's outermost nodes increases gradually from both ends to the center along the length direction. And in the center of the roller curve, the axial stress reaches its maximum. It shows that the plastic deformation occurs in Section III along the length direction.

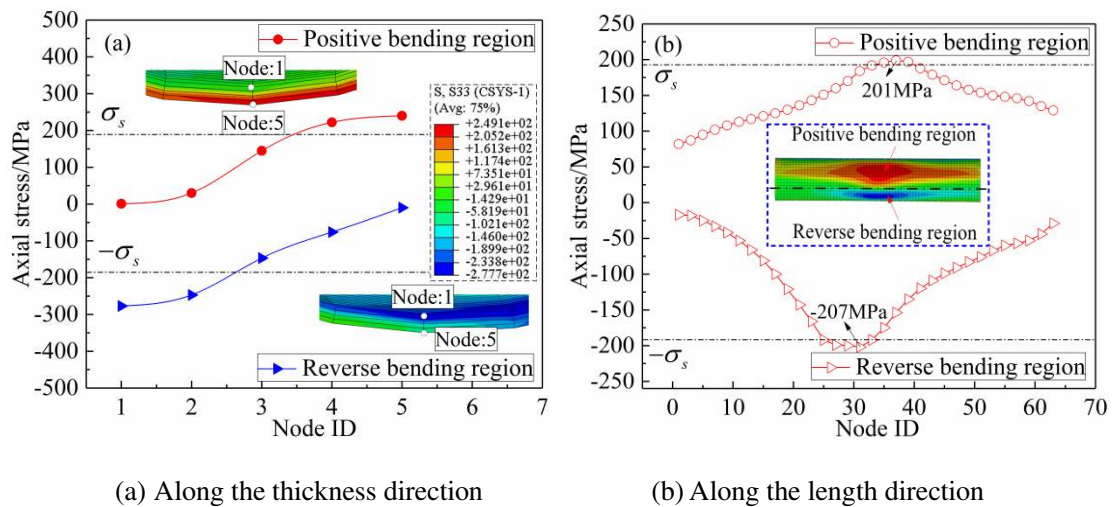


Fig. 11 Distribution of axial stress

The distribution of tangential stress along the thickness and circumferential directions in Section III is shown in Fig. 12. As indicated in Fig. 12, plastic deformation occurs along the thickness and circumferential directions under the influence of circumferential stress. It is proved that the geometric dimension of the circumferential section of the pipe has changed.

Fig. 12 (a) shows the distribution of circumferential stress along the thickness direction. In the positive bending region, the pipe's outer layer is stretched with a maximum stress of 287 MPa

(node 5); The inner layer are compressed with a minimum stress of -289 MPa (node 1). In the reverse bending region, the inner layer of the pipe is stretched, the maximum stress is 280 MPa (node 1); The outer layer is compressed, and the minimum stress is -276 MPa (node 5). From this, regardless of the positive bending region or the reverse bending region, the absolute value of the circumferential stress of the outer and inner of the pipe is basically the same.

Fig. 12 (b) shows the distribution of circumferential stress along the circumferential direction. The circumferential stress values of the pipe's outermost nodes are selected. As can be seen from Fig. 12 (b), the area of the positive bending region is larger than that of the reverse bending region. This is consistent with the equivalent stress distribution in Fig. 9. The absolute value of circumferential stress reaches the maximum at each region's center, and gradually decreases from the center to both ends.

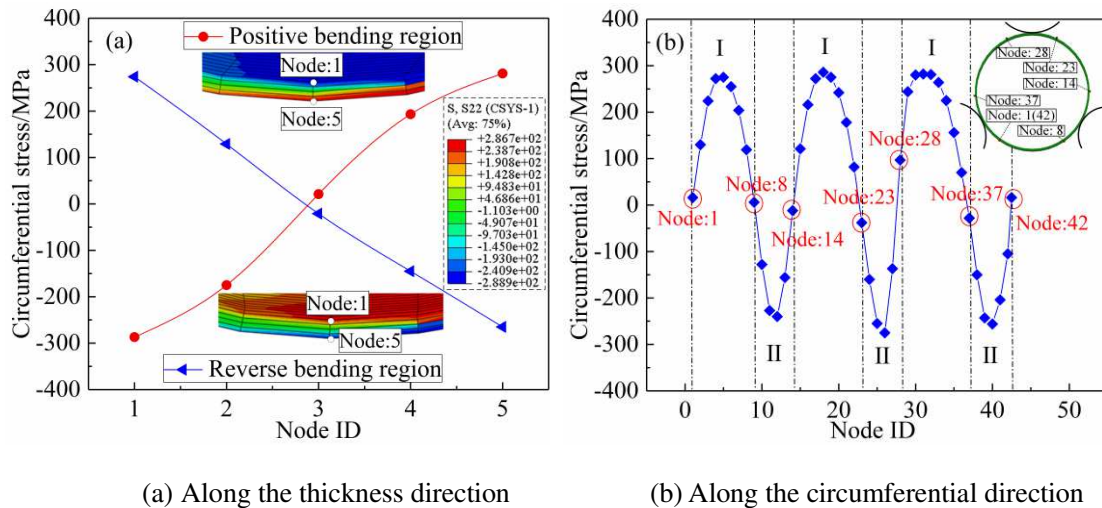


Fig. 12 Distribution of tangential stress (I: Positive bending region; II: Reverse bending region)

The distribution of radial stress in Section III is shown in Fig. 13. Fig. 13 shows that the radial stress of the pipe is very small, about -2.0 MPa to 2.0 MPa, and only elastic deformation occurs.

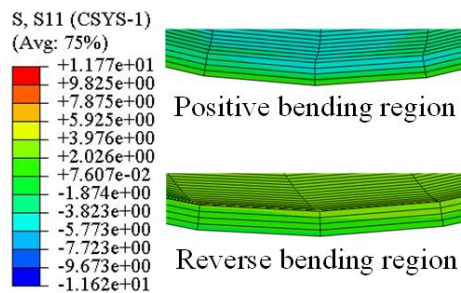


Fig. 13 Distribution of radial stress

The influence of axial stress, circumferential stress and radial stress on the calibration process of pipes is discussed by numerical simulation methods. The results show that the realization of the pipe calibration process is mainly influenced by the synergy between axial stress and circumferential stress. As a result, the simulation results also support the theoretical analysis results.

The equivalent stress distribution of ST12 pipe after calibration is shown in Fig. 14. It can be observed in Fig. 14 that the distribution of equivalent stress tends to be uniform and the residual stress is small.

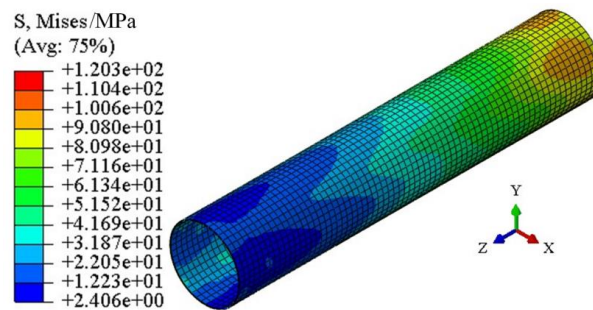


Fig. 14 Distribution of equivalent stress after calibration

5 Conclusions

(1) Theoretically, the reciprocating bending springback analysis of axial straightening and circumferential rounding are established respectively. The deformation mechanism of the process is revealed. It is proved that the reciprocating bending can eliminate the difference of initial curvature, and unify the axial and circumferential curvature to the same direction and value. It provides theoretical support for the calibration process to be applied to actual production.

(2) When the loading curvature tends to zero, the axial curvature after reciprocating bending is also close to zero. The straightness can be calibrated. When the loading curvature tends to a certain value, the circumferential curvature after reciprocating bending tends to be consistent. The roundness can be calibrated. The combination of axial reciprocating bending and circumferential reciprocating bending enables the calibration process of LSAW pipes.

(3) The simulation results show that the distribution of the maximum and minimum principal stress accord with the characteristics of pure bending deformation; After unloading and springback,

the residual stress of the pipe is small and evenly distributed; The calibration process is mainly influenced by the synergy of axial stress and circumferential stress, which further supports the theoretical analysis results.

Acknowledgments The authors would like to thank the National Natural Science Foundation of China and National Natural Science Foundation of Hebei province for their financial support.

Authors contributions **Xueying Huang:** Conceptualization, Methodology, Validation, Formal analysis, Investigation, Data curation, Writing - original draft, Writing - review & editing, Software, Visualization.

Gaochao Yu: Conceptualization, Methodology, Formal analysis, Supervision, Writing - review & editing.

Chunge Wang: Conceptualization, Methodology, Formal analysis, Supervision.

Jun Zhao: Conceptualization, Methodology, Formal analysis, Supervision.

Funding This project was funded and supported by National Natural Science Foundation of China [grant number 52005431], and National Natural Science Foundation of Hebei province [grant number E2020203086].

Compliance with ethical standards

Conflict of interests The authors declare that there is no conflict of interests regarding the publication of this paper.

Ethical approval The authors declare that this manuscript was not submitted to more than one journal for simultaneous consideration. Also, the submitted work is original and not have been published elsewhere in any form or language.

Consent to participate and publish The authors declare that they participated in this paper willingly and the authors declare to consent to the publication of this paper.

References

1. Deng D, Murakawa H, Liang W (2008) Numerical and experimental investigations on welding residual stress in multi-pass butt-welded austenitic stainless-steel pipe. *Computational Materials Science* 42(2): 234-244. [DOI: 10.1016/j.commatsci.2007.07.009](https://doi.org/10.1016/j.commatsci.2007.07.009)
2. Law M, Prask H, Luzin V, Gnaeupel-Herold T (2006) Residual stress measurements in coil linepipe and girth welded pipe. *Materials Science and Engineering A* 437(1): 60-63. [DOI:](https://doi.org/10.1016/j.msea.2005.08.009)

[10.1016/j.msea.2006.04.062](https://doi.org/10.1016/j.msea.2006.04.062)

3. Yaghi A, Hyde TH, Becker AA, Sun W, Williams JA (2008) Residual stress simulation in thin and thick-walled stainless steel pipe welds including pipe diameter effects. *International Journal of Pressure Vessels and Piping* 83(11-12): 864-874. DOI: [10.1016/j.ijpvp.2006.08.014](https://doi.org/10.1016/j.ijpvp.2006.08.014)
4. ANSI/API Specification 5L, Specification for line pipe (forty-fifth edition). Washington DC, United States, 2012.
5. Yin J, Zhao J, Qu XY, Zhai RX (2011) Springback analysis of expanding and setting round for large diameter pipe. *Journal of Mechanical Engineering* 47(12): 32-42. DOI: [10.3901/JME.2011.12.032](https://doi.org/10.3901/JME.2011.12.032)
6. Yin J, Zhao J, Sun HL, Zhan PP (2011) Precise compression and setting round by mould for large pipes. *Optics and Precision Engineering* 19(9): 2072-2078. DOI: [10.3788/OPE.20111909.2072](https://doi.org/10.3788/OPE.20111909.2072)
7. Zhao J, Zhan PP, Ma R, Zhai RX (2012) Control strategy of over-bending setting round for pipe-end of large pipes by mould press type method. *Transactions of Nonferrous Metals Society of China* 22(S2): 329-334. DOI: [10.1016/S1003-6326\(12\)61727-0](https://doi.org/10.1016/S1003-6326(12)61727-0)
8. Zhao J, Zhan PP, Ma R, Zhai RX (2013) Quantitative prediction of reduction in large pipe setting round process. *Chinese Journal of Mechanical Engineering (English Edition)* 26(4): 722-729.
9. Zhao J, Zhan PP, Ma R, Zhai RX (2014) Prediction and control of springback in setting round process for pipe-end of large pipe. *International Journal of Pressure Vessels and Piping* 116(1): 56-64. DOI: [10.1016/j.ijpvp.2014.01.006](https://doi.org/10.1016/j.ijpvp.2014.01.006)
10. Yu GC, Zhao J, Zhai RX, Ma R, Wang CG (2018) Theoretical analysis and experimental investigations on the symmetrical three-roller setting round process. *International Journal of Advanced Manufacturing Technology* 94(12): 45-56. DOI: [10.1007/s00170-016-9610-4](https://doi.org/10.1007/s00170-016-9610-4)
11. Zhao J, Yu GC, Ma R (2016) A mechanical model of symmetrical three-roller setting round process: The static bending stage. *Journal of Materials Processing Technology* 231: 501-512. DOI: [10.1016/j.jmatprotec.2016.01.002](https://doi.org/10.1016/j.jmatprotec.2016.01.002)
12. Yu GC, Zhao J, Xing JJ, Zhao FP, Li SL (2017) Research on the symmetrical three-roller setting round process. *Journal of Mechanical Engineering* 53(14): 136-143. DOI: [10.3901/JME.2017.14.136](https://doi.org/10.3901/JME.2017.14.136)
13. Zhao J, Song XK (2014) Control strategy of multi-point bending one-off straightening process for LSAW pipes. *International Journal of Advanced Manufacturing Technology* 72(9-12): 1615-1624.

DOI: 10.1007/s00170-014-5776-9

14. Zhao J, Song XK, Cao HQ, Liu J (2014) Press straightening control strategy of multi-step three-point bending for LSAW pipes. *Journal of Harbin Institute of Technology* 46(1): 90-96. DOI: 10.11918/j.issn.0367-6234.2014.01.016
15. Zhao J, Song XK, Cao HQ, Liu J (2014) Principle of multi-point bending one-off straightening process for longitudinally submerged arc welding pipes. *Journal of Mechanical Engineering* 50(2): 92-97. DOI: 10.3901/JME.2014.02.092
16. Yu GC, Zhai RX, Zhao J, Ma R (2018) Theoretical analysis and numerical simulation on the process mechanism of two-roller straightening, *International Journal of Advanced Manufacturing Technology* 94(9): 4011-4021. DOI: 10.1007/s00170-017-1120-5
17. Liu ZJ, Ma LD, Li JH, Du YK, Meng ZJ (2020) Accuracy analysis of six skewed-roll straightening process of tube. *Journal of Iron and Steel Research* 32(9): 55-61. DOI: 10.13228/j.boyuan.issn1001-0963.20200014
18. Wang CG, Yu GC, Wang W, Zhao J (2018) Deflection detection and curve fitting in three-roll continuous straightening process for LSAW pipes. *Journal of Materials Processing Technology* 255: 150-160. DOI: 10.1016/j.jmatprotec.2017.11.060
19. Wang CG, Zhang ZY, Zhai RX, Yu GC, Zhao J (2018) Cross-sectional distortion of LSAW pipes in over-bend straightening process. *Thin-Walled Structures* 129(AUG.): 85-93. DOI: 10.1016/j.tws.2018.03.016
20. Cui F, Yang HL (2015) New understanding in the field of straightening theory. *Heavy Machinery* 2-5. DOI:10.3969/j.issn.1001-196X.2015.01.001
21. Huang XY, Yu GC, Zhai RX, Ma R, Zhou C, Gao CL, Zhao J (2021) Roller design and numerical simulation of three-roller continuous and synchronous adjusting straightness and roundness process on LSAW pipes. *Journal of Mechanical Engineering* 57(10): 148-159. DOI: 10.3901/JME.2021.10.148
22. Huang XY, Yu GC, Zhao J, Mu ZK, Zhang ZY, Ma R (2020) Numerical simulation and experimental investigations on a three-roller setting round process for thin-walled pipes. *International Journal of Advanced Manufacturing Technology* 107: 355-369. DOI: 10.1007/s00170-020-05087-2
23. Huang XY, Zhao J, Yu GC, Meng QD, Zhai RX (2021) Three-roller continuous setting round

- process for longitudinally submerged arc welding pipes. Transactions of Nonferrous Metals Society of China 31(5): 1411-1426. [DOI: 10.1016/S1003-6326\(21\)65586-3](https://doi.org/10.1016/S1003-6326(21)65586-3)
24. Zhao J, Yu GC, WANG HR (2017) A roller-type continuous and synchronous calibrating straightness and roundness equipment and processing method for pipes. Hebei: CN106623507A, 2017-05-10.
25. Zhao J, Cao HQ, Zhan PP, Ma R (2012) Pure bending equivalent principle for over-bend straightening and its experimental verification. Journal of Mechanical Engineering 48(8): 28-33. [DOI: 10.3901/JME.2012.08.028](https://doi.org/10.3901/JME.2012.08.028)
26. Zhao J, Yin J, Ma R, Ma LX (2011) Springback equation of small curvature plane bending. Science China Technological Sciences 54: 2386-2396. [DOI: 10.1007/s11431-011-4447-4](https://doi.org/10.1007/s11431-011-4447-4)